Data Packet Structure and Modem Design for Dynamic Underwater Acoustic Channels

Y. Zakharov[1], B. Henson[1], R. Diamant[2], Y. Fei[3], P. D. Mitchell[1], N. Morozs[1], L. Shen[1], T. Tozer[1]

[1]Department of Electronic Engineering, University of York, UK

[2]Department of Marine Technologies, University of Haifa, Israel

[3]Key Laboratory of Underwater Acoustic Communication & Marine Information Technology,

Xiamen University, Ministry of Education, China

Abstract

In underwater acoustic (UWA) communications, the propagated signal undergoes severe Doppler and multipath distortions. The Doppler estimation/compensation and channel estimation/equalization techniques required to deal with these distortions contribute significantly to the overall complexity of UWA modems. In this paper, we propose a data packet structure for high data rate transmission in time-varying UWA channels with the channel dynamic modelled by velocity and acceleration between the transmitter and receiver. The data packet consists of superimposed data and periodic pilot sequences. The superposition allows achievement of a high spectral efficiency for data transmission. The repeated pilot symbols allow the use of a low-complexity multi-branch autocorrelation method for coarse estimation of Doppler parameters related to the velocity and acceleration. To refine these estimates, we further propose a low-complexity fine Doppler estimator based on dichotomous iterations. We also present a low complexity frequency domain channel estimator exploiting the channel sparsity. The proposed modem design has been evaluated using simulation and practical sea trials. The experiments demonstrate high detection performance of the proposed design, in particular in comparison with a more traditional design that ignores the acceleration between the transmitter and receiver.

Index Terms

Channel estimation, data packet, Doppler estimation, low complexity, sparse channel, time varying channel, underwater acoustic communication.

I. INTRODUCTION

In underwater acoustic (UWA) communications, the propagated signal experiences severe multipath and Doppler distortions. The Doppler estimation, channel estimation and equalization techniques significantly contribute to the high complexity of UWA modems. Such complexity may depend upon the signal waveform structure. Modems with multicarrier modulation, such as Orthogonal Frequency Division Multiplexing (OFDM) [2]–[5], exhibit good performance and relatively low complexity channel estimation and equalization, as most of the signal processing is performed in the frequency domain. However, OFDM signals are sensitive to Doppler distortions in the channel, thus requiring complicated Doppler estimators [6]. OFDM signals also have a high peak to average power ratio (PAPR), which places severe demands on the power amplifier at the transmitter. Single-carrier transmission on the other hand is less sensitive to the Doppler effect and has lower PAPR. There are accurate and computationally efficient Doppler estimators proposed for single-carrier transmission in UWA channels, e.g. see [7]–[12]. These techniques are used for fine Doppler estimation and correction in the receiver. Such estimation is applied after the data packet has been detected and initial coarse (yet still sufficiently accurate) Doppler estimates have been obtained.

One of most accurate methods for the initial coarse Doppler estimation in multipath UWA channels is based on computing the cross-ambiguity function (CAF) between the received and transmitted signals [13]–[15]. The CAF is computed on a two-dimensional (2D) grid of channel delay and Doppler compression factor. The position of the maximum CAF magnitude on the Doppler grid provides an estimate of the Doppler compression due to the transmitter/receiver velocity. However, a large number of Doppler estimation channels are required, which make the CAF method computationally intensive, even if the fast Fourier transform (FFT) and a two-step (coarse and fine estimation) approach are used to speed up the computations [5], [16], [17]. The CAF method is based on the assumption that the compression factor is time-invariant over the observation time interval, and therefore it may result in errors in scenarios with time-varying compression factor, e.g., due to transmitter/receiver acceleration.

In [18], [19], a technique based on computation of multi-branch autocorrelation (MBA) was proposed that provides accurate estimates of the Doppler compression caused by the transmitter/receiver velocity and acceleration and that requires significantly fewer computations than the CAF method. In this paper we exploit the MBA Doppler estimator and propose:

- a data packet structure that allows design of low-complexity modems operating in dynamic propagation environments, in particular for high data rate transmission;

- an example modem design for the proposed data packet structure, that can be implemented on real-time design platforms;

- a low-complexity channel estimator for multipath sparse channels and a low-complexity fine Doppler estimator.

We also present results from simulation and sea trials that illustrate excellent detection performance of the proposed design, in particular in comparison with the performance of a design using the more traditional approach to the Doppler estimation, based on computation of single-branch autocorrelation (SBA) [13], [17], [20]–[22], that ignores the acceleration.

The paper is organized as follows. Section II introduces the proposed structure of the transmitted data packet. Section III describes the channel model. The receiver design is presented in Section IV with the frequency domain sparse channel estimator and the fine Doppler estimator presented in subsections IV-A and IV-B, respectively. Section V describes simulation and sea experiments. Section VI concludes the paper.

II. Structure of the transmitted data packet

In dynamic UWA channels, the complexity of Doppler estimation represents a substantial part of the overall complexity of the receiver. The Doppler estimation normally refers to the estimation of the time compression factor of the received signal compared to the transmitted signal. In practice, such estimation is often implemented by computing the CAF between the received and transmitted (pilot) signals or the SBA of the received signal, or their variants. The CAF estimator provides a higher accuracy, while the SBA estimator is less complicated. Note that both the estimation approaches are based on the assumption that the time compression factor is constant over an observation interval. This assumption may be applicable when the transmitter and receiver are moving with constant speeds in a time-invariant environment. In highly dynamic environments and/or with a non-zero acceleration between the transmitter and receiver, this assumption is not valid.

In [19], a multi-branch autocorrelation (MBA) Doppler estimator was proposed, which has been shown to offer performance similar to that of the CAF method in application to OFDM signals recorded in sea experiments, while being significantly less complicated. The MBA estimator is an extension of the SBA estimator; it estimates the Doppler time compression not only due to transmitter/receiver velocity but also due to the acceleration. This is achieved by introducing several processing branches in a similar way to the computation in the CAF method, but with fewer branches and thus with lower complexity.

In the CAF method, the number of processing branches N_d is defined by the maximum speed v_M between the transmitter and receiver. More specifically, $N_d = \gamma v_M$, where $\gamma = f_c/(c\Delta_f)$, f_c is the carrier frequency, $c = 1500$ m/s is the sound speed, Δ_f is a Doppler frequency step (typically chosen as $\Delta_f = 1/\Theta$), and Θ is the signal duration. In the MBA method, the number of processing branches is defined by the maximum acceleration a_M between the transmitter and receiver. More specifically, it is given by $N_d = \gamma \Delta_v$, where Δ_v is the maximum variation of the speed between the transmitter and receiver over the signal duration Θ: $\Delta_v = a_M \Theta$. Since, for most practical scenarios, $\Delta_v \ll v_M$, and the complexity of processing in a single branch is almost the same for both the CAF and MBA methods, the MBA method is significantly less complicated. However, the MBA estimator requires a specific structure of transmitted signals, namely, the signal should be repeated within the observation interval.

Another consideration, when deciding on the data packet structure, is the efficient use of available time-frequency resources to achieve a high spectral efficiency. In practice, data transmission requires pilot signals and guard intervals, which can occupy a substantial part of the resources. The UWA channel is highly frequency-selective due to the wide delay spread of multipaths, and this requires dense pilot transmission in frequency. In highly dynamic (time-varying) UWA channels, dense pilot transmission in time is also necessary. Therefore, the resources left for the data transmission are significantly reduced.

The superimposed transmission of the data and pilot signals in the same frequency bandwidth and in the same time interval, on the other hand, completely avoids wasting the time-frequency resources, though the energy resources are still required for transmitting the pilot signal. Such combining requires half of the signal energy to be allocated to the pilot, i.e., half of signal energy can be considered as wasted. The channel capacity however is proportional to the logarithm of the signal energy, whereas it is directly proportional to the available frequency bandwidth. Therefore, it is considered beneficial if the pilot does not waste the time-frequency resources. See more discussion on using resources in the superimposed transmission in [5], [23]–[25].

This approach however requires signal processing techniques in the receiver to cancel the self-interference from the data when estimating the channel and from the pilot signal when demodulating the data. The self-interference can be efficiently dealt with using turbo-iterations. This has been shown in application to multi-carrier transmission [5]. Section IV describes the self-interference cancellation in the turbo-iterations and Section V shows its efficiency in the proposed modem.

In the data packet, the transmitted signal $s(t)$ represented by its samples $s(i)$ at a sampling frequency f_s is given by

$$s(i) = \Re \left\{ e^{j2\pi(f_c/f_s)i} \sum_{n=0}^{N-1} d_p(n) g \left(i - n \frac{f_s}{F_d} \right) \right\}, \tag{1}$$

where $d_p(n)$ is a sequence of superimposed data and pilot symbols, N the number of symbols in the data packet, $g(i)$ a pulse-shaping waveform, f_c the carrier frequency, F_d the symbol rate, and $\Re\{\cdot\}$ denotes the real part of a complex number.

In our example design, the superimposed symbols in the data packet are generated as

$$d_p(n) = p(n) + jd(n), \quad n = 0, \ldots, N-1, \tag{2}$$

where $p(n)$ and $d(n)$ are pilot and data symbols, respectively, and $j = \sqrt{-1}$. In the receiver, the pilot symbols $p(n)$ are used for Doppler estimation, channel estimation, time synchronization, and estimation of the signal-to-noise ratio (SNR) in diversity branches. The pilot symbol sequence is given by

$$p(n) = p_0(n) + p_0(n - N_p), \quad n = 0, \ldots, N-1, \tag{3}$$

where $p_0(n)$ is a pseudo-noise sequence of length $N_p = N/2$, $p_0(n) = 0$ for $n < 0$ and $n > N_p - 1$, and $p_0(n)$ and $d(n)$ are BPSK symbols with values ± 1. More generally, the symbols $p(n)$ and $d(n)$ in (2) can be taken from different QAM constellations.

To ease understanding of further material in this paper, here we present parameters of an example data packet:

- the carrier frequency $f_c = 24$ kHz;

- the sampling frequency $f_s = 96$ kHz;

- the symbol rate $F_d = 6 \times 10^3$ symbols/s; thus, the original data rate is 6 kbps;
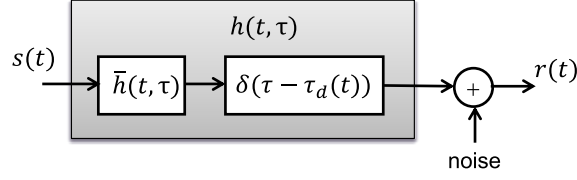
Fig. 1. Representation of the channel as a time-variant filter.

126   • the pulse shaping waveform $g(i)$, $i = -L_{\text{RRC}}, \ldots, L_{\text{RRC}}$ of length $2L_{\text{RRC}} + 1$ is the impulse response of the

127   truncated root-raised cosine (RRC) filter [26], $L_{\text{RRC}} = 80$; the RRC roll-off factor [26] $\alpha = 0.2$ and thus the

128   frequency bandwidth of the transmitted signal is $(1 + \alpha)F_d = 7.2$ kHz;

129   • $N = 6000$, so that the packet duration is $\Theta = 1.00167$ s, of which 0.00167 s accounts for the length of the

130   pulse-shaping waveform;

131   • convolutional coding at a code rate $1/2$ with polynomials $(561, 753)$ in octal [27] is applied to the transmitted

132   data to generate the data sequence $d(n)$; thus, a single data packet carries 3 kbits of useful data.

133   In our experiments, we will be using this and some other data packet examples. Note that other data and pilot

134   signals, including multi-carrier signals, can be used with such a data packet structure.

III. CHANNEL MODEL

136   The UWA channel is often modelled as a time-variant linear system with an impulse response $h(t, \tau)$ that describes

137   both the multipath and Doppler spread. The noise-free signal at the receiver input is given by

$$y(t) = \int_{-\infty}^{\infty} h(t, \tau)s(t - \tau)d\tau, \tag{4}$$

138   and the received signal $r(t)$ is given by

$$r(t) = y(t) + n(t), \tag{5}$$

139   where $n(t)$ is a noise signal. To recover the transmitted signal, the receiver should equalize the channel. With a fast

140   moving transmitter and/or receiver, direct equalization of the fast-varying impulse response $h(t, \tau)$ is complicated.

141   In these scenarios, another approach is used.

142   The dynamic UWA channel can be represented using two time-varying components, described by a fast-time-

143   varying channel delay $\tau_d(t)$ and a slower-time-varying channel impulse response $\bar{h}(t, \tau)$, as shown in Fig. 1 [5],

[19], [28]. This channel representation is often implicitly used for designing UWA receivers [2], [6], [8], [29]. The time-variant delay line described by the impulse response $\delta(\tau - \tau_d(t))$, where $\delta(\tau)$ is the Dirac delta function, is associated with the fastest channel variations caused by the varying distance between the transmitter and the receiver. However, it can be described by a few parameters, and therefore reliably estimated using a coarse Doppler estimator. In practice, this channel component is equalized via resampling, by introducing a compensating delay $-\tau_d(t)$ into the received signal, i.e., essentially the resampling is represented as a time-variant delay line with the impulse response $\delta(\tau + \tau_d(t))$. However, different multipath components of the received signal experience different variations in their delays, i.e., different time-compressions. Therefore, the resampled received signal still contains residual Doppler distortions. These distortions are described in Fig. 1 by the component with the impulse response $\bar{h}(t, \tau)$. This channel component incorporates differential variations in the lengths of acoustic rays due to the transmitter/receiver movement, and it is typically slower varying in time than the impulse response $h(t, \tau)$. In some cases, this component can be assumed to be time-invariant over the data packet.

The delay $\tau_d(t)$ over an interval of interest is often represented as a linear function of time [3], [4], [17]:

$$\tau_d(t) = a_0 + a_1 t, \tag{6}$$

where a_0 is a constant delay, normally associated with the time difference between the transmitter and receiver; and with perfect time synchronization, $a_0 = 0$. The parameter a_1 is associated with a constant velocity v between the transmitter and receiver, and, more specifically, $a_1 = v/c$, where c is the sound speed (e.g., $c = 1500$ m/s). However, for highly dynamic movements of the transmitter and/or receiver, the linear model of $\tau_d(t)$ in (6) becomes inaccurate.

A more accurate model is given by [19]

$$\tau_d(t) = a_0 + a_1 t + a_2 t^2, \tag{7}$$

where $a_1 = v/c$ and v is the initial velocity at $t = 0$, a_2 is associated with the acceleration a between the transmitter and receiver, and more specifically, $a_2 = a/(2c)$. We will show that, even in moderately dynamic UWA channels, the receiver developed using the model (7) can significantly outperform one based on the model (6).

The second component of the channel representation, described by the impulse response $\bar{h}(t, \tau)$, contains many parameters to be estimated, such as the multipath delays and complex amplitudes. However, these parameters are
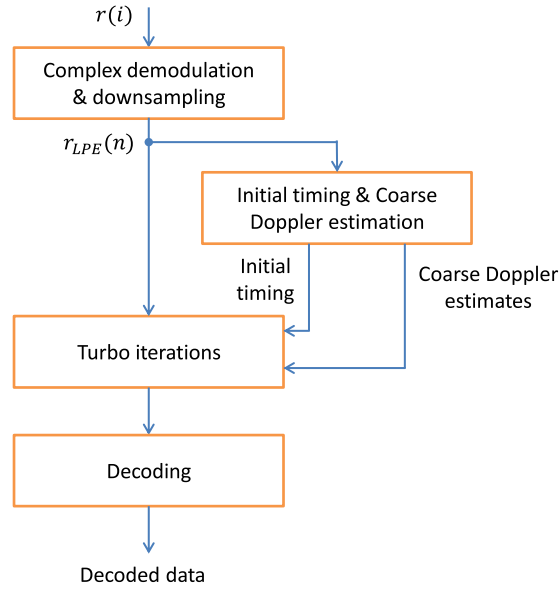
Fig. 2. General structure of the receiver. The received signal $r(t)$ is represented by samples $r(i)$ at the high sampling frequency f_s; the low-pass equivalent (LPE) signal is represented by samples $r_{\text{LPE}}(n)$ at the lower sampling frequency F_{ds}.

168   usually more slowly varying in time compared to the channel response $h(t, \tau)$. Consequently, equalization of this

169   channel component is easier than the direct equalization of $h(t, \tau)$.

170   In the receiver, we will model $\tau_d(t)$ as in (7). To simplify the signal processing algorithms in the receiver, they

171   are developed assuming that $\bar{h}(t, \tau) = \bar{h}(\tau)$ is time invariant over the packet duration. However, when testing the

172   modem (see Section V), this assumption may not be applied to the UWA channel in the test.

173   <div align="center">IV. RECEIVER</div>

174   The general structure of the receiver is shown in Fig. 2. The signal processing is performed at two sampling

175   rates. The highest sampling rate f_s is chosen to avoid distortions due to the analog-to-digital conversion of the

176   received passband signal: $f_s > 2f_c + (1 + \alpha)F_d$. The complex demodulation transforms the passband signal into

177   a baseband (low-pass equivalent (LPE)) signal with overall bandwidth $(1 + \alpha)F_d$ at the lower sampling rate F_{ds},

178   which, in our design, is set to $F_{ds} = 2F_d$.

179   The coarse Doppler estimation, based on the MBA method, provides estimates of the Doppler parameters a_1

180   and a_2 for reasampling the LPE signal in the turbo iterations. It also provides the timing synchronization for

windowing the received data for further processing in the turbo iterations. After the turbo iterations, the equalized

and demodulated symbols are decoded. Details of the processing are presented below.

1) Complex demodulation and downsampling: The input signal $r(t)$ to the receiver is represented by real-valued

samples $r(i)$ at the sampling rate f_s. The LPE signal samples are computed as:

$$r_{\text{LPE}}(n) = \sum_{i=-L_{\text{RRC}}}^{L_{\text{RRC}}} g(i)r(i - nK)e^{-j2\pi(f_c/f_s)(i-nK)}, \tag{8}$$

where $K = f_s/F_{ds}$ is the downsampling factor and n is the time index at the sampling rate F_{ds}.

In our realization, this processing requires about 2×10^6 real-valued MAC (multiply/accumulate) [30], [31]

operations per second. This takes into account that the RRC filter has 161 taps and there are F_{ds} samples per

second. This also takes into account the specific ratio $f_s = 4f_c$, for which the real and imaginary parts of the

complex exponential in (8) have 50% zeros and the remaining values are ± 1. Note that low-power DSP processors

can provide 200×10^6 MACs per second, e.g., see [32], therefore this processing can be easily implemented in real-

time. More advanced DSP processors have FIR-accelerators [33] for efficient implementation of the computation

in (8). This stage can also be comfortably implemented on an FPGA platform [34].

2) Initial timing and coarse Doppler estimation: This processing is based on the MBA Doppler estimator [19].

Its core function is the computation of the 2D autocorrelation function of the signal $r_{\text{LPE}}(n)$ on the grid of delay

τ and frequency shift F for every time instant n:

$$A_{\text{MBA}}(\tau, F, n) =$$

$$\sum_{q=n-QN_p+1}^{n} r_{\text{LPE}}^*(q)r_{\text{LPE}}\left(q + \frac{\tau}{\Delta_\tau}\right)e^{j2\pi F\Delta_\tau q}, \tag{9}$$

where $\frac{\tau}{\Delta_\tau} \in \{QN_p - \frac{\tau_M}{\Delta_\tau}, QN_p - \frac{\tau_M}{\Delta_\tau}\}$, $Q = F_{ds}/F_d = 2$, $F = m\Delta_f$, $m = -N_a, \ldots, N_a$, Δ_τ is the delay step, and

Δ_f is the frequency step on the grid; we set $\Delta_\tau = 1/F_{ds}$ and $\Delta_f = 1/\Theta$. The parameter τ_M is chosen to guarantee

$\tau_M > v_M/(cQN_p)$, where v_M is the maximum speed between the transmitter and receiver. The parameter N_a is

chosen to guarantee $N_a > \Theta f_c a_M/(2c\Delta_f)$, where a_M is the maximum acceleration between the transmitter and
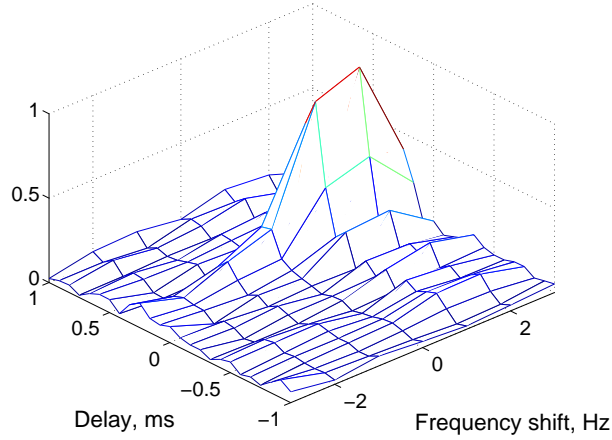
receiver.

Fig. 3. 2D autocorrelation in a multipath channel with $v = 1$ m/s and $a = 0.2$ m/s^2 at the moment corresponding to the maximum in Fig. 4; SNR = 20 dB. The data packet parameters are as presented in Section II. Grid resolution: $\Delta_f = 1$ Hz, $\Delta_\tau = 1/F_{ds} = 83.3$ μs.

Let

$$I(n) = \max_{\tau, F} |A_{\text{MBA}}(\tau, F, n)|, \tag{10}$$

$$n_{\max} = \arg\max_n I(n), \tag{11}$$

$$\{\tau_{\max}, F_{\max}\} = \arg\max_{\tau, F} |A_{\text{MBA}}(\tau, F, n_{\max})|. \tag{12}$$

Then estimates of the parameters a_1 and a_2 in the Doppler model (7) are given, respectively, by [19]

$$\hat{a}_1 = 1 - \frac{\Theta}{2\tau_{\max}} + \frac{F_{\max}}{2f_c}, \tag{13}$$

$$\hat{a}_2 = \frac{F_{\max}}{2\tau_{\max} f_c}. \tag{14}$$

An example of $|A_{\text{MBA}}(\tau, F, n_{\max})|$ is shown in Fig. 3. The maximum of the 2D autocorrelation is shifted in delay and frequency with respect to the center of the delay-frequency plane. The delay and frequency shifts are proportional to the velocity v and acceleration a between the transmitter and receiver. The center of the grid corresponds to no time compression due to the velocity (delay axis) or acceleration (frequency axis). The peak extracted from the autocorrelation function, as shown in Fig. 3, is further interpolated to improve the estimation accuracy; the interpolation is similar to that in [5].

The autocorrelation function in Fig. 3 corresponds to the maximum of $I(n)$ shown in Fig. 4. The position ($n_{\max}$) of the maximum in Fig. 4 is treated as an estimate of the temporal center of the data packet, thus providing the time synchronisation.
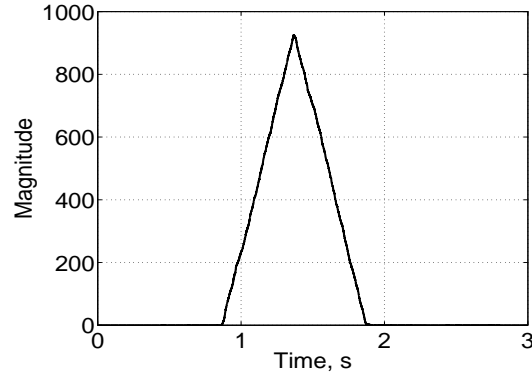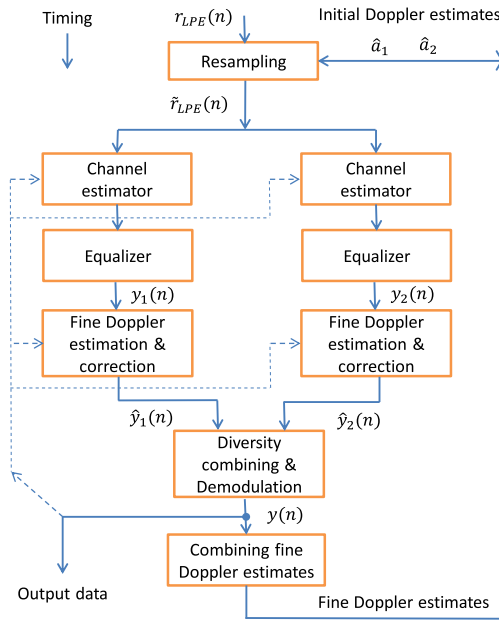
Fig. 4. Function $I(n)$ with the maximum at $n_{\max}$.

Fig. 5. Turbo-iterations in the receiver.

For our example design, these computations require about 30×10^6 MACs/s. This allows computation of 280 2D autocorrelation values to cover the velocity range $v \in [-5, 5]$ m/s and acceleration range $a \in [-0.25, 0.25]$ m/s^2 at the sampling rate $F_{ds} = 12$ kHz. The computation of $A_{\mathrm{MBA}}(\tau, F, n)$ in (9), representing the highest complexity, can be comfortably implemented on an FPGA platform.

216   *3) Turbo-iterations:* The block diagram of processing in one of N_{it} turbo iterations is shown in Fig. 5. The

217   input LPE signal $r_{\mathrm{LPE}}(n)$ is resampled according to the estimate of $\tau_d(t)$:

$$\hat{\tau}_d(t) = \hat{a}_0 + \hat{a}_1 t + \hat{a}_2 t^2, \tag{15}$$

218   where $\hat{a}_0$ is the timing estimate. At the first iteration, estimates $\hat{a}_1$ and $\hat{a}_2$, obtained via interpolation of the peak of

219   the 2D autocorrelation function $|A_{\mathrm{MBA}}(\tau, F, n_{\max})|$, are used for the resampling. At further iterations, these estimates

220   are refined by the fine Doppler estimator (see subsection IV-B). The resampled signal is denoted as $\tilde{r}_{\mathrm{LPE}}(n)$.

221   There are two branches of processing, with even samples of $r_{\mathrm{LPE}}(n)$ processed in the 'left' branch and the odd

222   samples processed in the 'right' branch (see Fig. 5). Otherwise, the two branches perform the same processing.

223   The two processing branches relate to oversampling by a factor of two ($F_{ds} = 2F_d$) in our design. It is possible

224   to use the single branch, i.e., $F_{ds} = F_d$. The work in [5] shows that the detection performance of the receiver in

225   this case is significantly inferior to that in the case of the oversampling $F_{ds} = 2F_d$. However, further oversampling,

226   e.g., $F_{ds} = 4F_d$ does not bring a significant improvement in the performance, while making the receiver more

227   complicated. Therefore, in our design, we use two processing branches.

228   The channel estimation and equalization are performed in the frequency domain to reduce the complexity (see

229   subsection IV-A). The fine Doppler estimation and correction (see subsection IV-B) are applied to equalized symbols

230   $y_b(n)$, $n = 0, \ldots, N-1$. The Doppler corrected symbols $\hat{y}_b(n)$ are combined according to

$$y(n) = w_1 \hat{y}_1(n) + w_2 \hat{y}_2(n), \tag{16}$$

231   and demodulated. The weights w_1 and w_2 ($0 \leq w_b \leq 1$) for the (maximal-ratio) combining are computed based on

232   SNR estimates in the branches,

$$\mathrm{SNR}_b = \frac{1}{N} \sum_{n=0}^{N-1} \left[\Re\{\hat{y}_b(n)\} - p(n) \right]^2, \quad b = 1, 2. \tag{17}$$

233   The weights are then found as:

$$w_b = \frac{\sqrt{\mathrm{SNR}_b}}{\sqrt{\mathrm{SNR}_1} + \sqrt{\mathrm{SNR}_2}}. \tag{18}$$

234   The estimate in (17) is based on the fact that, in the case of perfect equalization, the real part of the signal $\hat{y}_b(n)$

235   should only contain the pilot signal $p(n)$. Any difference from $p(n)$ can be treated as a noise. Since the pilot energy

236   is equal to N, SNR_b is a ratio of the noise energy estimate to the signal energy, i.e., an estimate of SNR in the

237   b-th branch.

238   The fine Doppler estimates found in the two branches are also combined using the same weights:

$$
\begin{cases}
\hat{a}_1 = w_1 \hat{a}_{1,1} + w_2 \hat{a}_{1,2} \\
\hat{a}_2 = w_1 \hat{a}_{2,1} + w_2 \hat{a}_{2,2}
\end{cases}
\tag{19}
$$

239   where $\hat{a}_{1,b}$ and $\hat{a}_{2,b}$ are estimates of the Doppler parameters a_1 and a_2, respectively.

240   Algorithm 1 in Appendix A summarizes the main signal processing steps in the turbo iterations.

241   The main contribution into the complexity of turbo iterations comes from the channel estimation and equalization.

242   These however can be efficiently implemented as presented in subsection IV-A.

A. Frequency domain channel estimation using sparse basis of complex exponentials

244   In the conference paper [1], we proposed to use in this modem a frequency-domain BEM (Basis Expansion

245   Model) channel estimator based on B-splines as the basis functions. This low-complexity estimator provides a high

246   accuracy if the delay spread in the channel is small compared to the data packet length. For larger delay spreads,

247   the number of basis functions should be increased thus leading to higher channel estimation errors. The number

248   of basis functions can be reduced if the channel is sparse. However, typical UWA channels are not sparse in the

249   B-spline space.

250   They are however often relatively sparse in the space of complex exponentials. Channel estimators exploiting

251   the sparsness are well described in the literature [3], [35]–[38]. In this section, we present a low-complexity sparse

252   channel estimator. The proposed estimator, as will be shown in our experiments, has a high enough estimation

253   accuracy to provide reliable demodulation of the data packet.

254   Note that the sparse estimation can be done in two steps. The first step is to find a support Γ, or in other

255   words, a set of basis functions essentially contributing into representation of the channel frequency response. This

256   is equivalent to finding delays of multipath components with significant magnitudes. The second step is to find the

257   expansion coefficients for the basis functions in the support, or in other words, to estimate complex amplitudes of

258   the essential multipaths.

259   In the first step, even if more basis functions are chosen into the support than an 'oracle' algorithm could provide,

260   we can still achieve good channel estimation performance, as long as this number is not excessive (comparable to

261   the true number of non-zero multipath components in the channel). Therefore, the support estimation is based on

262   searching the maxima of the cross-correlation function of the received and transmitted signals as follows.

Let samples of the Doppler corrected LPE signal at the symbol rate F_d in the two processing branches be represented as

$$\tilde{z}_b(n) = \tilde{r}_{\text{LPE}}[2(n - N_p - n_{\max}) + b], \quad b = 1, 2, \tag{20}$$

where $n_{\max}$ is found in (11). These samples are then transformed into the frequency domain using the FFT:

$$Z_b(k) = \sum_{n=0}^{N_{\text{FFT}}-1} \tilde{z}_b(n) e^{-j2\pi kn/N_{\text{FFT}}}. \tag{21}$$

The size N_{FFT} is chosen high enough to cover the length N of the data packet together with possible channel delay spread and time synchronization errors; as long as this condition is satisfied, the value of N_{FFT} does not affect the receiver performance, although longer N_{FFT} results in a higher complexity. In the example design of the modem, we set $N_{\text{FFT}} = 8192 > 6000 = N$.

The pilot signal $p(n)$ and tentatively demodulated data symbols $\tilde{d}(n)$, $n = 0, \ldots N - 1$, are combined into estimates of the transmitted symbols, $\tilde{d}_p(n) = p(n) + j\tilde{d}(n)$, and transformed into the frequency domain:

$$P(k) = \sum_{n=0}^{N_{\text{FFT}}-1} \tilde{p}(n) e^{-j2\pi kn/N_{\text{FFT}}}, \tag{22}$$

where

$$\tilde{p}(n) = \begin{cases} 0, & n - \frac{N_{\text{FFT}}}{2} < -N_p \\ \tilde{d}_p(n - \frac{N_{\text{FFT}}}{2} + N_p), & -N_p < n - \frac{N_{\text{FFT}}}{2} < N_p \\ 0, & n - \frac{N_{\text{FFT}}}{2} > N_p \end{cases} \tag{23}$$

At the first turbo iteration, $\tilde{d}(n) = 0$. At subsequent iterations, $\tilde{d}(n) = 0$ if $\Im[y(n)] < \beta$ and $\tilde{d}(n) = \text{sign}\{\Im[y(n)]\}$ if $\Im[y(n)] \geq \beta$, where $\Im[\cdot]$ denotes an imaginary part of a complex number; in our design, we set $\beta = 0.25$.

The cross-correlation function of the received and transmitted signals is computed as

$$\gamma_b(n) = \frac{1}{N_{\text{FFT}}} \sum_{k=0}^{N_{\text{FFT}}-1} Z_b(k) P^*(k) e^{j2\pi kn/N_{\text{FFT}}}. \tag{24}$$

The first up to M maxima of $|\gamma_b(n)|^2$ for $n \in [N_{\text{FFT}} - \Upsilon, N_{\text{FFT}}] \vee [0, \Upsilon]$, exceeding a threshold $t_{\text{paths}} = \kappa \max_n |\gamma_b(n)|^2$, where $0 < \kappa < 1$ and we use $\kappa = 4 \cdot 10^{-4}$, determine the support Γ of a cardinality $|\Gamma| = M_{\max} \leq M$. The parameter Υ defines the maximum delay spread $[-\Upsilon/F_d, \Upsilon/F_d]$ in the channel. With $\Upsilon = 1000$, used in our design, as high channel delay spread as 330 ms is covered by the estimator.

In the second step, the expansion coefficients are found using the regularized least squares algorithm as follows. Denote

$$\mathbf{B}^{(q)} = \left\{ e^{-j2\pi k m(q)/N_{\text{FFT}}} \right\}_{k=0}^{N_{\text{FFT}}-1}, \quad m(q) \in \Gamma, \tag{25}$$

an $N_{\text{FFT}} \times 1$ vector, representing the qth column of the $N_{\text{FFT}} \times M_{\max}$ basis matrix $\mathbf{B}$, where $m(q)$ represents the channel delay of the qth path in the support Γ. Denote $\mathbf{P} = \text{diag}\{[P(0), \ldots, P(N_{\text{FFT}} - 1)]^T\}$. The $M_{\max} \times 1$ vector $\hat{\mathbf{c}}_b$ of expansion coefficients is found by solving the $M_{\max} \times M_{\max}$ system of equations

$$\mathbf{G}_b \hat{\mathbf{c}}_b = \boldsymbol{\xi}_b, \tag{26}$$

where

$$\mathbf{G}_b = \mathbf{B}^H \mathbf{P}^H \mathbf{P} \mathbf{B} + \varepsilon \mathbf{I}, \tag{27}$$

$$\boldsymbol{\xi}_b = \mathbf{B}^H \mathbf{P}^H \tilde{\mathbf{z}}_b, \tag{28}$$

$\varepsilon > 0$ is a small number, $\mathbf{I}$ is the identity matrix, and $\tilde{\mathbf{z}}_b$ is a vector with elements $\tilde{z}_b(n)$ defined in (20). The channel frequency response is then estimated as the BEM [39]:

$$\hat{\mathbf{h}}_b = \mathbf{B} \hat{\mathbf{c}}_b. \tag{29}$$

With the frequency response $\hat{h}_b(k)$ (elements of the vector $\hat{\mathbf{h}}_b$), and received signal in the frequency domain $Z_b(k)$, the spectrum of the equalized signal is given by

$$Y_b(k) = \frac{Z_b(k)\hat{h}_b^*(k)}{\hat{h}_b(k)^2 + \eta}, \quad k = 0, \ldots, N_{\text{FFT}} - 1, \tag{30}$$

where $\eta > 0$ is a small number used to prevent division by zero. Finally, the equalized signal $y_b(n)$ in branch b is obtained by applying the inverse FFT to $Y_b(k)$.

The complexity of the channel estimator is mainly due to computation of the matrix $\mathbf{G}_b$ in (27), which, when implemented using a matrix-by-matrix multiplication, requires $2N_{\text{FFT}}M^2$ MACs. Notice that the matrix $\mathbf{G}_b$ is well structured and its elements $G_{p,q}$ are given by

$$G_{p,q} = \sum_{k=0}^{N_{\text{FFT}}-1} |P(k)|^2 e^{-j2\pi k |m(q)-m(p)|/N_{\text{FFT}}}. \tag{31}$$

Therefore, by pre-computing (by using FFT)

$$\rho(n) = \sum_{k=0}^{N_{\text{FFT}}-1} |P(k)|^2 e^{-j2\pi k n/N_{\text{FFT}}}, \tag{32}$$

elements of $\mathbf{G}_b$ can be found as

$$G_{p,q} = \rho(|m(q) - m(p)|). \tag{33}$$

With such an approach, the complexity of computing $\mathbf{G}_b$ is only $3\log(N_{\text{FFT}})N_{\text{FFT}}$ MACs, if using the split-radix

FFT algorithm [40] for computation as in (32). Moreover, the computation in (32) needs to be done only once for

both the branches, whereas (27) is computed twice. Thus, the complexity is reduced by about $4M^2/[3\log(N_{\text{FFT}})]$

times. In many practical scenarios, the value of M is not very high; in our case, $M = 40$ was good enough for all

experiments. With $M = 40$ and $N_{\text{FFT}} = 8192$, the reduction in complexity is by 160 times.

The direct solution of the system in (26) requires $\mathcal{O}(M^3)$ MACs [41], which is not high compared to the

computation of $\mathbf{G}_b$. However, this may involve square root operations, not well suited to implementation on DSP

processors and FPGAs. To reduce the complexity and make the algorithm suitable for implementation on fixed-point

DSP and hardware platforms, the DCD (dichotomous coordinate descent) algorithm can be used [42], [43]. Note

that elements of the vector $\boldsymbol{\xi}_b$ in (28) are elements of $\gamma_b(n)$ at the support Γ, and they are already available.

The computation of the channel estimate in (29), if using the direct matrix-vector multiplication, would require

$4MN_{\text{FFT}}$ MACs. If using the FFT, it is reduced to $3\log(N_{\text{FFT}})N_{\text{FFT}}$ MACs. With $M = 40$ and $N_{\text{FFT}} = 8192$, the

complexity reduction is by 4 times.

Thus, the complexity of the channel estimation and equalization in one branch within one turbo iteration is

approximately equivalent to 4 FFTs, the support Γ estimation, which requires about $2M\Upsilon$ MACs, and solving

the system of equations. As an example, with $M = 40$, $\Upsilon = 1000$ and $N_{\text{FFT}} = 8192$, the complexity is about

1.5×10^6 MACs. Resampling can be based on the local cubic splines [44], and its complexity is also small

compared to the complexity of the other signal processing. Thus, with $N_{it} = 5$, used in all our experiments, the

overall complexity of turbo iterations is about 15×10^6 MACs. The use of FFTs can be especially beneficial for

implementation on some DSP platforms, where FFT-accelerators are available [33].

B. Fine Doppler estimation

After the initial Doppler compensation, there is still a residual Doppler distortion. The fine Doppler estimation

is performed after equalization of the LPE signal in the branches.

Let $y_b(n)$ be the equalised symbols in branch b, and $\tilde{d}_p(n)$ be the same as in (23). We assume the following signal model describing the residual Doppler distortion:

$$y_b(n) = d_p(n)e^{j2\pi(f_{e,b}+a_{e,b}n)n}. \tag{34}$$

The fine Doppler estimation deals with estimation of the parameters $f_{e,b}$ and $a_{e,b}$, and it is based on the dichotomous frequency estimation [45], [46] and a similar dichotomous algorithm for fine estimation of linear-in-time dependence of the frequency. These are algorithms with negligible complexity compared to the complexity of the other signal processing in the receiver.

Denote $\tilde{y}_b(n) = y_b(n)\tilde{d}_p^*(n)$. In the estimator of $f_{e,b}$, at every dichotomous iteration, the following quantities are computed (starting from $f_{e,b} = 0$ in the first iteration):

$$\begin{aligned} C_i &= \sum_{n=0}^{N-1} \tilde{y}_b(n)e^{-j2\pi(f_{e,b}+i\delta_f)n}, \\ i_{\max} &= \arg\max_{i=-1,0,+1}\{|C_i|^2\}. \end{aligned} \tag{35}$$

If $i_{\max} = -1$, then $f_{e,b}$ is updated as: $f_{e,b} \leftarrow f_{e,b} - \delta_f$, else if $i_{\max} = +1$, then $f_{e,b} \leftarrow f_{e,b} + \delta_f$. After the update, the step-size δ_f is reduced by half (thus the name *dichotomous*): $\delta_f \leftarrow \delta_f/2$. We set the initial step-size to $\delta_f = 1/N$ and use 8 dichotomous iterations. After completing the iterations, the frequency estimate $f_{e,b}$ is used to compensate the residual velocity:

$$\bar{y}_b(n) = \tilde{y}_b(n)e^{-j2\pi f_{e,b}n}. \tag{36}$$

In the estimator of $a_{e,b}$, at every dichotomous iteration, the following quantities are computed (starting from $a_{e,b} = 0$ in the first iteration):

$$\begin{aligned} D_i &= \sum_{n=0}^{N-1} \bar{y}_b(n)e^{-j2\pi(a_{e,b}+i\delta_a)n^2}, \\ i_{\max} &= \arg\max_{i=-1,0,+1}\{|D_i|^2\}. \end{aligned} \tag{37}$$

If $i_{\max} = -1$, then $a_{e,b} \leftarrow a_{e,b} - \delta_a$, else if $i_{\max} = +1$, then $a_{e,b} \leftarrow a_{e,b} + \delta_a$. After the update, the step-size δ_a is reduced: $\delta_a \leftarrow \delta_a/2$. We set the initial step-size to $\delta_a = 1/N^2$ and use 8 dichotomous iterations. After completing the iterations, the estimate $a_{e,b}$ is used to compensate the residual acceleration:

$$\hat{y}_b(n) = \bar{y}_b(n)e^{-j2\pi a_{e,b}n^2}. \tag{38}$$

TABLE I

COMPLEXITY OF MAIN BLOCKS OF THE RECEIVER IN THE EXAMPLE DESIGN (MACS PER SECOND).

Complex demodulation & downsampling	Coarse Doppler estimation	Turbo iterations	Total complexity
2×10^6	30×10^6	15×10^6	47×10^6

The signals $\hat{y}_b(n)$ are used for the diversity combining in (16). The estimates of the Doppler parameters a_1 and a_2 are updated as

$$\hat{a}_{1,b} \leftarrow \hat{a}_{1,b} + f_{e,b}\frac{F_d}{f_c}, \tag{39}$$

$$\hat{a}_{2,b} \leftarrow \hat{a}_{2,b} + a_{e,b}\frac{F_d^2}{f_c}. \tag{40}$$

The fine Doppler estimates are used in the current turbo iteration to provide additional Doppler correction in (36) and (38), which compensates for a residual Doppler effect still present in the processed signal. The extra Doppler correction engenders an improvement in the detection performance. The fine Doppler estimates obtained in the two branches are combined as in (19) and used in the next turbo iteration for more accurate resampling.

The Doppler estimation is performed at several stages of signal processing in the receiver. Algorithm 2 in Appendix B summarizes the Doppler estimation in the receiver.

C. Receiver complexity

Table I summarizes the receiver complexity (without the decoding) for the example design. It can be seen that the coarse Doppler estimation dominates the complexity. The receiver (without the decoding) requires less than 50×10^6 MACs per second, which is affordable for implementation on most modern low-power DSP processors.

V. SIMULATION AND SEA TRIALS

This section describes simulation and sea trials. Subsection V-A presents simulation results and subsection V-B presents results of a sea trial.
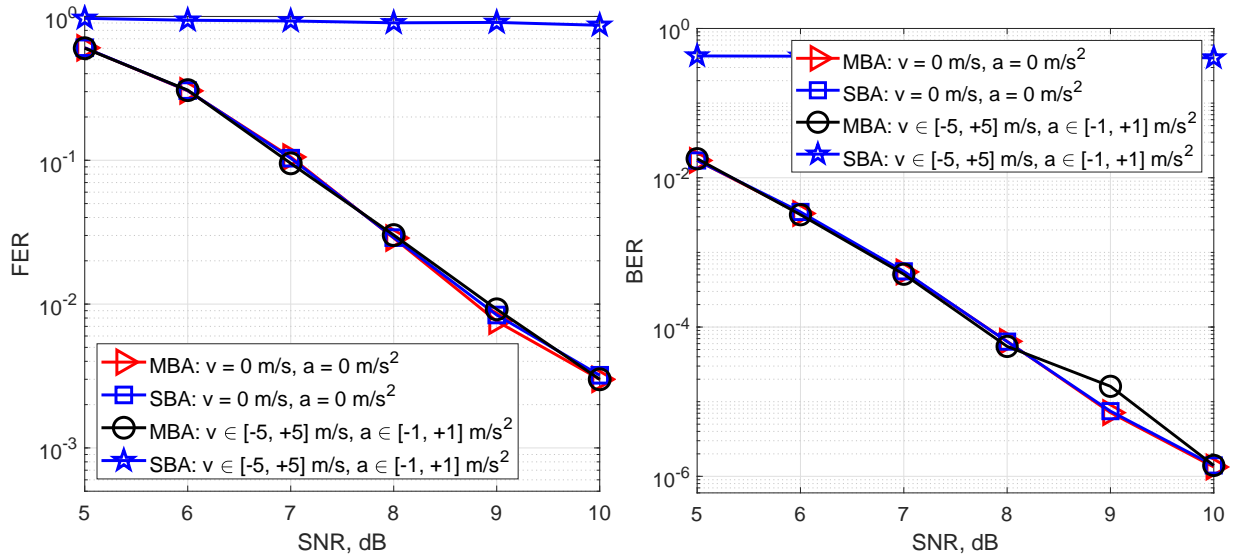
Fig. 6. Detection performance of the proposed receiver with the MBA and SBA Doppler estimators in the channel with a static multipath component $\bar{h}(t,\tau)$ (see Fig. 1). The time varying delay $\tau_d(t)$ is caused by the velocity v and acceleration a as given by (7).

A. Numerical experiments

This subsection presents numerical simulation results. We first consider the simulation in a channel (see Fig. 1) with a time-varying delay $\tau_d(t)$, while the multipath structure described by the impulse response $\bar{h}(t,\tau) = \bar{h}(\tau)$ is time-invariant. This model is an exact match to the channel model used for designing the modem.

In the second simulation, we use the Waymark channel model [28], implementing the virtual signal transmission [47] in specified underwater acoustic environments with specified motion of the transmitter and receiver, with both $\tau_d(t)$ and $\bar{h}(t,\tau)$ varying in time. The Waymark simulator is based on computation of the underwater acoustic field using the ray tracing software Bellhop [48]. Parameters of the rays are transformed into a set of channel impulse responses at samples (waymarks) of the transmitter/receiver trajectory. The waymark impulse responses are interpolated in time to compute the time varying channel impulse response $h(t,\tau)$ for every sample of the transmitted signal. The convolution of the transmitted signal and channel impulse response produces the noise-free received signal.

1) Experiments with static multipath structure: In this simulation, the channel model consists of a linear system representing a static multipath channel followed by a time Doppler compression that is defined by a velocity v and acceleration a. The channel power delay profile (PDP) is defined by delays $[1, 11, 43, 91, 100]/F_{ds}$ and uniform

path variances. In a single simulation trial, the velocity and acceleration are the same for all paths. Two scenarios

are considered: (i) $v = 0$ m/s, $a = 0$ m/s^2; (ii) v is random and uniformly distributed within $[-5, +5]$ m/s, a is

random and uniformly distributed within $[-1, +1]$ m/s^2; i.e., in different simulation trials these values are different.

For this simulation, the example modem design is used with parameters presented in Section II. The SBA estimator

is implemented as the MBA estimator with $N_a = 0$.

Fig. 6 shows the frame error ratio (FER), computed as the ratio of the number of data packets received with

errors in 5000 simulation trials to the total number of packets. It also shows the bit error ratio (BER). It can be seen

that the receiver with the SBA Doppler estimator cannot operate in the second scenario, where the acceleration is

not zero. However, both the SBA and MBA estimators show similar performance for the first scenario ($v = 0$ m/s,

$a = 0$ m/s^2), which perfectly matches to the SBA estimator. It is also seen that the receiver with the MBA Doppler

estimator provides consistently high detection performance in channels with various Doppler distortions.

2) Waymark experiment: We consider the SWellEx-96 (Event S5) acoustic environment [49] (see also [28]) with

the sea depth 220 m. The receiver is positioned 1 m above the sea bottom. The transmitter is positioned above

the receiver 1 m below the sea surface and moves synchronously with the surface waves. The surface waves are

described as a 2D-sinusoid of 3 m amplitude with a time period of 8 s, and space period of 100 m. The transmit

antenna beampattern is a cone of $\pm\, 45°$ with the look direction towards the receiver. The multipath channel structure

is mostly defined by the direct and first bottom-reflected paths as can be seen in Fig. 7. There are also clusters of

multipaths with delays around 0.3 s, 0.6 s, etc., with respect to the direct path, arriving at the receiver after multiple

reflections from the sea surface and sea bottom; however, they have significantly reduced magnitudes and therefore

do not affect the receiver performance.

In the experiment, lasting about 14 s, 8 data packets are transmitted. Parameters of the data packet are: $f_c =$

12 kHz; $f_s = 48$ kHz; $F_d = 2$ kHz; $\Theta = 0.5$ s. The received signal (without noise) is shown in Fig. 8. We have

then run 5000 simulation trials, adding to this signal a different realization of white noise in each trial, to evaluate

the effect of SNR on the receiver performance.

Fig. 9 shows the FER performance averaged over the 8 data packets. It can be seen that the receiver with the

MBA Doppler estimator shows good performance, whereas the receiver with the SBA estimator cannot operate in
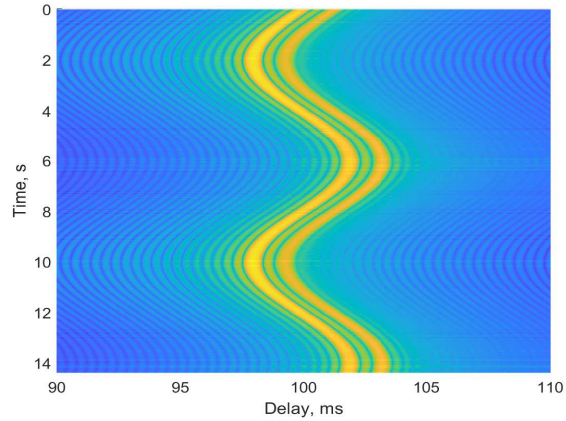
this scenario.

Fig. 7. Time-varying impulse response for the vertical transmission from the time-varying sea surface to the bottom at a depth of 220 m.
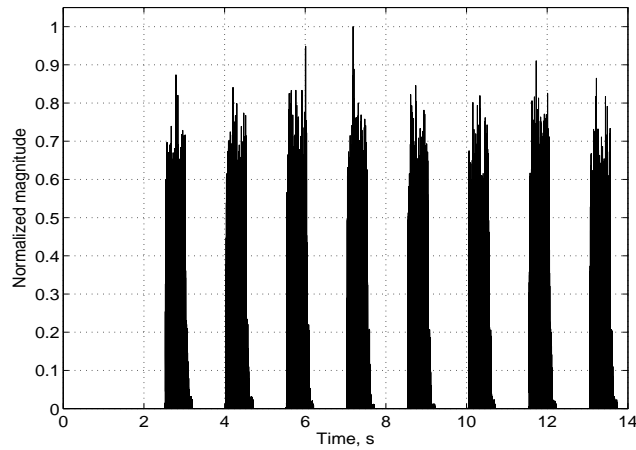

Fig. 8. Noise-free magnitude of the received signal in the Waymark experiment in the Swellex environment with moving surface.

B. Sea experiment

The sea experiment was conducted roughly one mile across the shores of Haifa, Israel, with the sea depth 12 m. In the experiment, a light motorboat was moving away from the receiver with a transducer deployed at a depth of about 2 m. For the transmitter, the software defined EvoLogics LF modem was used [50]. The receiving hydrophone was mounted on an anchored buoy at a depth of 8 m. The sound speed profile was measured to be flat at roughly 1543 m/s, the wind speed was about 1 knot. In the experiment, the received signal was recorded and later processed off-line.

During 80 s of the experiment, the distance between the transmitter and receiver increased from about 100 m
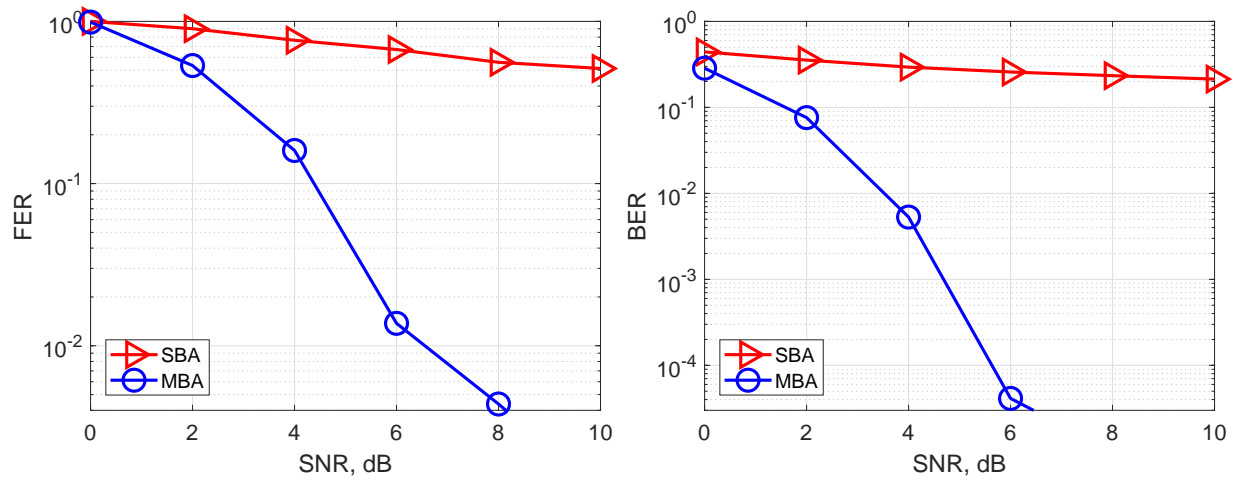
Fig. 9. FER and BER performance of the receiver in the experiment in the Swellex environment with vertical transmission and moving sea surface.
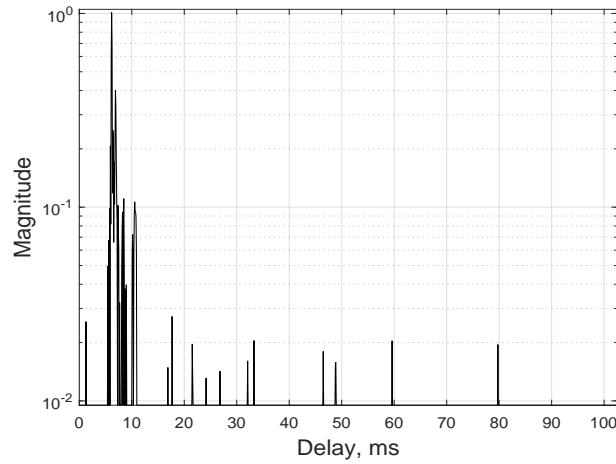

Fig. 10. Impulse response estimate obtained in the sea experiment.

to 200 m, and 15 data packets were transmitted. Parameters of the data packet are: $f_c = 12.5$ kHz; $f_s = 96$ kHz; $F_d = 6.25$ kHz; $\Theta = 0.8$ s. The typical impulse response in the experiment is shown in Fig. 10.

The moving motorboat was affected by surface waves of about 0.5 m amplitude, which resulted in varying velocity and acceleration as illustrated in Fig. 11. The results in Fig. 11 were obtained using the proposed receiver. To validate the measurements, they were repeated for another receiving hydrophone 0.45 m away from the first one; the measurements in both cases are very close.

Fig. 12 shows the BER (Bit Error Ratio) performance of the receiver with the MBA and SBA Doppler estimators.
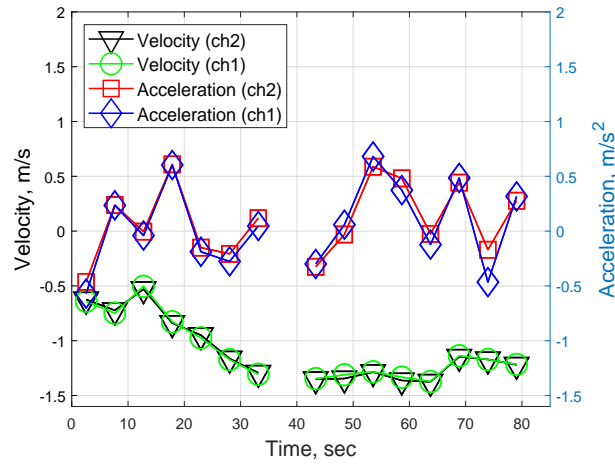
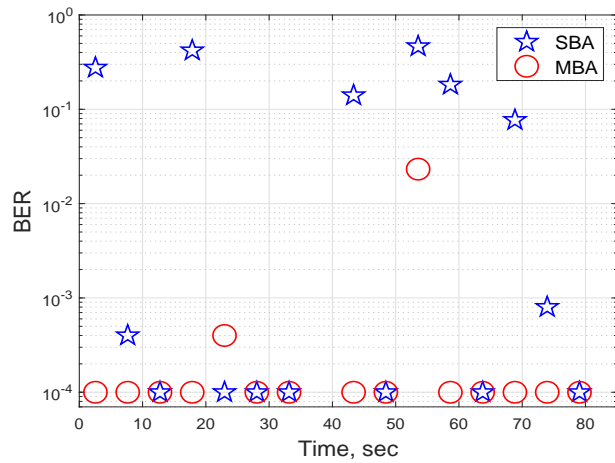Fig. 11. Estimates of the velocity and acceleration in the sea experiment.

Fig. 12. BER performance in the sea experiment.

The data packets received without errors are shown as having BER $= 10^{-4}$ (this is lower than the minimum BER $1/2500$, which can be measured over a single packet carrying 2500 data bits). It can be seen that the MBA estimator indeed outperforms the SBA estimator. From comparison of Fig. 12 and Fig. 11, it is seen that the benefit of using the MBA estimator is especially pronounced for data packets received at higher acceleration. Thus, even in these mild conditions (slow speed of the transmitter and relatively calm sea surface), it can be seen that taking the acceleration into account is very important for reliable data transmission.

VI. Conclusions

We have proposed a data packet structure for transmission in UWA channels. The superimposed data and pilot symbols in the packet allow high spectral efficiency of the data transmission. We have proposed a low-complexity receiver capable of dealing with the multipath propagation and the Doppler effect caused by the transmitter/receiver motion described by velocity and acceleration. The complexity analysis has shown that the example design (without the decoding) can be implemented with approximately 50×10^6 MAC operations per second. The Doppler estimator and channel estimator dominate the complexity of the receiver. The periodic structure of the pilot signal in the data packet allows the use of the computationally efficient multi-branch autocorrelation method for the Doppler estimation. We have also proposed a low-complexity channel estimator exploiting the channel sparsity and fine Doppler estimator based on dichotomous iterations. Numerical simulation and sea experiments have shown a high detection performance of the proposed design, in particular in comparison with the performance of a design based on the more traditional approach to Doppler estimation that ignores the acceleration.

Acknowledgement

We would like to thank the reviewers for their very useful comments that allowed us to improve the paper.

Appendix A

Turbo-iterations

Algorithm 1 summarizes the main signal processing steps in the turbo iterations.

Algorithm 1: Turbo-iterations

---

input : signal $r_{\text{LPE}}(n)$; Doppler estimates $\hat{a}_1$, $\hat{a}_2$; timing estimate $\hat{a}_0$

output: signal $y(n)$; Doppler estimates $\hat{a}_1$, $\hat{a}_2$

1 while *number of iterations is less than N_{it}* **do**

2   Resample $r_{\text{LPE}}(n)$ into $\tilde{r}_{\text{LPE}}(n)$ using $\tau_d(t)$ from (15)

3   **for** $b \leftarrow 1, 2$ **do**

4   Extract $\tilde{z}_b(n)$, $n = 0, \ldots, N_{\text{FFT}} - 1$, from $\tilde{r}_{\text{LPE}}(n)$ as in (20)

5   Transform $\tilde{z}_b(n)$ into the frequency domain, $Z_b(k)$, $k = 0, \ldots, N_{\text{FFT}} - 1$, as in (21)

6   Find the frequency-domain channel estimate $\hat{\mathbf{h}}_b$ as in (29)

7   Equalize $Z_b(k)$ in the frequency domain to obtain $Y_b(k)$ as in (30)

8   Transform $Y_b(k)$ into the time domain $y_b(n)$, $n = 0, \ldots, N_{\text{FFT}} - 1$,

9   Find the fine Doppler estimates $\hat{a}_{1,b}$ and $\hat{a}_{2,b}$ as in (39) and (40)

10   Make the fine Doppler correction of $y_b(n)$ to obtain the signal $\hat{y}_b(n)$ as in (38)

11   Find the SNR estimate SNR_b as in (17)

12   **end**

13   Compute the weight coefficients w_1 and w_2 as in (18)

14   Produce the combined signal $y(n)$ from $\hat{y}_1(n)$ and $\hat{y}_2(n)$ as in (16)

15   Produce the new Doppler estimates $\hat{a}_1$ and $\hat{a}_2$ from $\hat{a}_{1,b}$ and $\hat{a}_{2,b}$ as in (19)

16 end

APPENDIX B

DOPPLER ESTIMATION IN THE RECEIVER

Algorithm 2 summarizes the Doppler estimation in the receiver.

Algorithm 2: Doppler estimation

---

input : 2D autocorrelation $A_{\mathrm{MBA}}(\tau, F, n_{\max})$; signal $r_{\mathrm{LPE}}(n)$

output: Doppler estimates $\hat{a}_1$, $\hat{a}_2$

1 Find the coarse Doppler estimates as follows.

2   (i) Find the peak $\{\tau_{\max}, F_{\max}\}$ of $|A_{\mathrm{MBA}}(\tau, F, n_{\max})|$ over τ and F as in (12)

3   (ii) Refine $\{\tau_{\max}, F_{\max}\}$, e.g., using the parabolic interpolation of the peak as described in [5]

4   (iii) Compute the coarse Doppler estimates $\hat{a}_1$ and $\hat{a}_2$ as in (13) and (14), respectively

5 **while** *number of iterations is less than N_{it}* **do**

6   Resample $r_{\mathrm{LPE}}(n)$ using $\hat{a}_1$ and $\hat{a}_2$ as in (15)

7   **for** $b \leftarrow 1, 2$ **do**

8   Find the fine Doppler estimates $\hat{a}_{1,b}$ and $\hat{a}_{2,b}$ as in (39) and (40), respectively

9   **end**

10   Produce the combined fine Doppler estimates $\hat{a}_1$ and $\hat{a}_2$ from $\hat{a}_{1,b}$ and $\hat{a}_{2,b}$ as in (19)

11 **end**

REFERENCES

[1] Y. Zakharov, Y. Fei, P. Mitchell, N. Morozs, B. Henson, L. Shen, and T. Tozer, "Low-complexity UAC modem and data packet structure," in *Fourth Underwater Communications and Networking Conference (UComms), Lerici, Italy*. IEEE, 28-30 Aug. 2018, pp. 1–5.

[2] B. Li, S. Zhou, M. Stojanovic, L. Freitag, and P. Willett, "Multicarrier communication over underwater acoustic channels with nonuniform Doppler shifts," *IEEE Journal of Oceanic Engineering*, vol. 33, no. 2, pp. 198–209, 2008.

[3] C. R. Berger, S. Zhou, J. C. Preisig, and P. Willett, "Sparse channel estimation for multicarrier underwater acoustic communication: From subspace methods to compressed sensing," *IEEE Transactions on Signal Processing*, vol. 58, no. 3, pp. 1708–1721, 2010.

[4] S. Yerramalli and U. Mitra, "Optimal resampling of OFDM signals for multiscale–multilag underwater acoustic channels," *IEEE Journal of Oceanic Engineering*, vol. 36, no. 1, pp. 126–138, 2011.

[5] Y. V. Zakharov and A. K. Morozov, "OFDM transmission without guard interval in fast-varying underwater acoustic channels," *IEEE Journal of Oceanic Engineering*, vol. 40, no. 1, pp. 144–158, 2015.

[6] S. Yoshizawa, T. Saito, Y. Mabuchi, T. Tsukui, and S. Sawada, "Variable range resampling for computationally efficient Doppler compensation in underwater acoustic communication," in *Proceedings of MTS/IEEE OCEANS*, 28 May, 2018, pp. 1–4.

[7] M. Stojanovic, J. A. Catipovic, and J. G. Proakis, "Phase-coherent digital communications for underwater acoustic channels," *IEEE Journal of Oceanic Engineering*, vol. 19, no. 1, pp. 100–111, 1994.

[8] M. Johnson, L. Freitag, and M. Stojanovic, "Improved Doppler tracking and correction for underwater acoustic communications," in *IEEE Int. Conf. Acoustics, Speech, and Signal Processing, ICASSP-97*, 1997, vol. 1, pp. 575–578.

[9] T. J. Riedl and A. C. Singer, "Broadband Doppler compensation: Principles and new results," in *Conference Record of the Forty Fifth Asilomar Conference on Signals, Systems and Computers (ASILOMAR)*, 2011, pp. 944–946.

[10] K. A. Perrine, K. F. Nieman, T. L. Henderson, K. H. Lent, T. J. Brudner, and B. L. Evans, "Doppler estimation and correction for shallow underwater acoustic communications," in *2010 IEEE Conference Record of the Forty Fourth Asilomar Conference on Signals, Systems and Computers*, pp. 746–750.

[11] R. Diamant, A. Feuer, and L. Lampe, "Choosing the right signal: Doppler shift estimation for underwater acoustic signals," in *Proceedings of the Seventh ACM International Conference on Underwater Networks and Systems*. ACM, 2012, p. 27.

[12] F. Qu, Z. Wang, L. Yang, and Z. Wu, "A journey toward modeling and resolving doppler in underwater acoustic communications," *IEEE Communications Magazine*, vol. 54, no. 2, pp. 49–55, 2016.

[13] G Jourdain, "Characterization of the Underwater Channel Application to Communication," in *Issues in Acoustic Signal-Image Processing and Recognition*, pp. 197–209. Springer, 1983.

[14] T. H. Eggen, A. B. Baggeroer, and J. C. Preisig, "Communication over Doppler spread channels. part I: Channel and receiver presentation," *IEEE Journal of Oceanic Engineering*, vol. 25, no. 1, pp. 62–71, 2000.

[15] T. Arikan, T. Riedl, A. Singer, and J. Younce, "Comparison of OFDM and single-carrier schemes for Doppler tolerant acoustic communications," in *IEEE OCEANS-2015, Genova*, 2015, pp. 1–7.

[16] B. Li, S. Zhou, M. Stojanovic, L. Freitag, and P. Willett, "Non-uniform Doppler compensation for zero-padded OFDM over fast-varying underwater acoustic channels," in *IEEE OCEANS 2007-Europe*, pp. 1–6.

[17] S. F. Mason, C. R. Berger, S. Zhou, and P. Willett, "Detection, synchronization, and Doppler scale estimation with multicarrier waveforms in underwater acoustic communication," *IEEE Journal on Selected Areas in Communications*, vol. 26, no. 9, pp. 1638–1649, 2008.

[18] Y. V. Zakharov and J. Li, "Autocorrelation method for estimation of Doppler parameters in fast-varying underwater acoustic channels," in *Underwater Acoustics, Conference and Exhibition, UACE-2015. Crete, Greece.*, 2015, pp. 1–4.

[19] J. Li, Y. Zakharov, and B. Henson, "Multibranch autocorrelation method for Doppler estimation in underwater acoustic channel," *IEEE Journal of Oceanic Engineering*, vol. 43, no. 4, pp. 1099–1113, 2018.

[20] S. M. Kay and S. B. Doyle, "Rapid estimation of the range-Doppler scattering function," *IEEE Transactions on Signal Processing*, vol. 51, no. 1, pp. 255–268, 2003.

[21] A. E. Abdelkareem, B. S. Sharif, C. C. Tsimenidis, J. A. Neasham, and O. R. Hinton, "Low-complexity Doppler compensation for OFDM-based underwater acoustic communication systems," in *IEEE OCEANS-2011, Spain*, 2011, pp. 1–6.

[22] A. E. Abdelkareem, B. S. Sharif, and C. C. Tsimenidis, "Adaptive time varying Doppler shift compensation algorithm for OFDM-based underwater acoustic communication systems," *Ad Hoc Networks*, vol. 45, pp. 104–119, 2016.

[23] M. Ghogho, D. McLernon, E. Alameda-Hernandez, and A. Swami, "Channel estimation and symbol detection for block transmission using data-dependent superimposed training," *IEEE Signal Processing Letters*, vol. 12, no. 3, pp. 226–229, 2005.

[24] J. K. Tugnait and X. Meng, "On superimposed training for channel estimation: performance analysis, training power allocation, and frame synchronization," *IEEE Transactions on Signal Processing*, vol. 54, no. 2, pp. 752–765, 2006.

[25] S. He and J. K. Tugnait, "On doubly selective channel estimation using superimposed training and discrete prolate spheroidal sequences," *IEEE Transactions on Signal Processing*, vol. 56, no. 7, pp. 3214–3228, 2008.

[26] G. L. Stuber, *Principles of Mobile Communication*, Kluwer Academic Publishers Norwell, MA, USA, 1996.

[27] J. G. Proakis, "Digital communications," *McGraw Hill, New York*, 1995.

[28] C. Liu, Y. V. Zakharov, and T. Chen, "Doubly selective underwater acoustic channel model for a moving transmitter/receiver," *IEEE Transactions on Vehicular Technology*, vol. 61, no. 3, pp. 938–950, 2012.

[29] S. Yerramalli and U. Mitra, "On optimal resampling for OFDM signaling in doubly-selective underwater acoustic channels," in *IEEE OCEANS'2008*, pp. 1–6.

[30] L. J. Karam, I. A. Kamal, A. Gatherer, G. Frantz, D. V. Anderson, B. L. Evans, et al., "Trends in multicore DSP platforms," *IEEE Signal Processing Magazine*, vol. 26, no. 6, pp. 38–49, 2009.

[31] A. Bateman and S. I. Paterson, *The DSP handbook*, Prentice-Hall, 2002.

[32] Texas Instruments, *TMS320C5545 Fixed-Point Digital Signal Processor*, 2016, http://www.ti.com/lit/ds/sprs853d/sprs853d.pdf.

[33] Analog Devices, "SHARC+ dual core DSP with ARM Cortex-A5," Dec 2018, https://www.analog.com/en/products/adsp-sc589.html.

[34] H. S. Dol, P. Casari, T. Van der Zwan, and R. Otnes, "Software-defined underwater acoustic modems: Historical review and the NILUS approach," *IEEE Journal of Oceanic Engineering*, vol. 42, no. 3, pp. 722–737, 2017.

[35] W. Li and J. C. Preisig, "Estimation of rapidly time-varying sparse channels," *IEEE Journal of Oceanic Engineering*, vol. 32, no. 4, pp. 927–939, 2007.

[36] J. Huang, C. R. Berger, S. Zhou, and J. Huang, "Comparison of basis pursuit algorithms for sparse channel estimation in underwater acoustic OFDM," in *in Proceedings of IEEE OCEANS 2010, Sydney*, 2010, pp. 1–6.

[37] C. Qi, X. Wang, and L. Wu, "Underwater acoustic channel estimation based on sparse recovery algorithms," *IET Signal Processing*, vol. 5, no. 8, pp. 739–747, 2011.

[38] N. U. R. Junejo, H. Esmaiel, M. Zhou, H. Sun, J. Qi, and J. Wang, "Sparse channel estimation of underwater TDS-OFDM system using look-ahead backtracking Orthogonal Matching Pursuit," *IEEE Access*, vol. 6, pp. 74389–74399, 2018.

[39] Y. Zakharov, T. Tozer, and D. Pearce, "Acoustic echo cancellation using frequency-domain spline identification," *IEEE Transactions on Signal Processing*, vol. 55, no. 2, pp. 585–593, 2007.

[40] P. Duhamel and H. Hollmann, "'Split-radix FFT algorithm," *Electronics Letters*, vol. 20, no. 1, pp. 14–16, 1984.

[41] G. H. Golub and C. F. Van Loan, *Matrix computations*, The Johns Hopkins University Press, Baltimore, 3rd edition, 1996.

[42] Y. V. Zakharov and T. C. Tozer, "Multiplication-free iterative algorithm for LS problem," *Electonics Letters*, vol. 40, no. 9, pp. 567–569, 2004.

[43] J. Liu, Y. V. Zakharov, and B. Weaver, "Architecture and FPGA design of dichotomous coordinate descent algorithms," *IEEE Trans. on Circuits and Systems I: Regular Papers*, vol. 56, no. 11, pp. 2425–2438, 2009.

[44] Y. V. Zakharov, T. C. Tozer, and J. F. Adlard, "Polynomial spline-approximation of Clarke's model," *IEEE Transactions on Signal Processing*, vol. 52, no. 5, pp. 1198–1208, 2004.

[45] Y. Zakharov and T. Tozer, "Frequency estimator with dichotomous search of periodogram peak," *Electronics Letters*, vol. 35, no. 19, pp. 1608–1609, 1999.

[46] Y. Zakharov, V. Baronkin, and T. Tozer, "DFT-based frequency estimators with narrow acquisition range," *IEE Proceedings-Communications*, vol. 148, no. 1, pp. 1–7, 2001.

[47] J. C. Peterson and M. B. Porter, "Ray/beam tracing for modeling the effects of ocean and platform dynamics," *IEEE Journal of Oceanic Engineering*, vol. 38, no. 4, pp. 655–665, 2013.

[48] Michael B Porter, "THE BELLHOP Manual and User's Guide: Preliminary draft," *Heat, Light, and Sound Research, Inc., La Jolla, CA, USA, Tech. Rep*, 2011.

[49] J. Murray and D. Ensberg, *The SWellEx-96 Experiment*, 1996, [Online] Available: http://www.mpl.ucsd.edu/swellex96/.

[50] "Specifications of the EvoLogics LF modem," Accessed: 08-01-2019, https://www.evologics.de/en/products/acoustics/s2cr_7_17.html.